



Design, synthesis, biochemical studies, cellular characterization, and structure-based computational studies of small molecules targeting the urokinase receptor

Fang Wang^a, W. Eric Knabe^a, Liwei Li^{a,b}, Inha Jo^a, Timmy Mani^a, Hartmut Roehm^a, Kyungsoo Oh^c, Jing Li^a, May Khanna^a, Samy O. Meroueh^{a,b,c,*}

^aIndiana University, Department of Biochemistry and Molecular Biology, Indiana University School of Medicine, Indianapolis, IN 46202, United States

^bCenter for Computational Biology and Bioinformatics, Indiana University School of Medicine, Indianapolis, IN 46202, United States

^cDepartment of Chemistry and Chemical Biology, Indiana University Purdue University Indianapolis (IUPUI), Indianapolis, IN 46202, United States

ARTICLE INFO

Article history:

Received 31 March 2012

Revised 25 May 2012

Accepted 1 June 2012

Available online 12 June 2012

Keywords:

Urokinase receptor

Small molecule inhibitors

Protein–protein interaction

Virtual screening

Structure–activity relationship

Metastasis

Lung cancer

Synthesis

Structure-based drug design

ABSTRACT

The urokinase receptor (uPAR) serves as a docking site to the serine protease urokinase-type plasminogen activator (uPA) to promote extracellular matrix (ECM) degradation and tumor invasion and metastasis. Previously, we had reported a small molecule inhibitor of the uPAR–uPA interaction that emerged from structure-based virtual screening. Here, we measure the affinity of a large number of derivatives from commercial sources. Synthesis of additional compounds was carried out to probe the role of various groups on the parent compound. Extensive structure-based computational studies suggested a binding mode for these compounds that led to a structure–activity relationship study. Cellular studies in non-small cell lung cancer (NSCLC) cell lines that include A549, H460 and H1299 showed that compounds blocked invasion, migration and adhesion. The effects on invasion of active compounds were consistent with their inhibition of uPA and MMP proteolytic activity. These compounds showed weak cytotoxicity consistent with the confined role of uPAR to metastasis.

© 2012 Elsevier Ltd. All rights reserved.

1. Introduction

The urokinase receptor (uPAR) is a cell-surface GPI-anchored protein that has been strongly implicated with tumor invasion and metastasis. The receptor is up-regulated in highly aggres-

Abbreviations: uPAR, urokinase receptor; uPA, urokinase-type plasminogen activator; suPAR, soluble urokinase receptor; MMP, matrix metalloproteinase; RTK, receptor tyrosine kinase; GPCR, G-protein coupled receptor; ECM, extracellular matrix; MAPK, mitogen-activated protein kinase; FAK, focal adhesion kinase; DMSO, dimethyl sulfoxide; FP, fluorescence polarization; FDA, food and drug administration; DNA, deoxyribonucleic acid; PBS, phosphate buffered saline; Src, sarcoma; MDA-MB-231, MD Anderson Metastatic Breast; FBS, fetal bovine serum; DMEM, Dulbecco's Modified Eagle Medium; SDS, sodium dodecyl sulfate; CBB, Coomassie brilliant blue; BSA, bovine serum albumin; FITC, fluorescein isothiocyanate; TBST, Tris-Buffered Saline and Tween 20; IB, immunoblot; NMR, nuclear magnetic resonance; DCM, dichloromethane; HRMS, high-resolution mass spectrometry; THF, tetrahydrofuran; PDB, protein databank; DMAP, 4-dimethylaminopyridine; DCC, *N,N'*-dicyclohexylcarbodiimide; FAM, 6-carboxyfluorescein; GPI, glycosylphosphatidylinositol; MTT, 3-(4,5-dimethylthiazol-2-yl)-2,5-diphenyltetrazolium bromide; HPLC, high-performance liquid chromatography; FN, fibronectin; ELISA, enzyme-linked immunosorbent assay.

* Corresponding author. Tel.: +1 317 274 8315; fax: +1 317 278 9217.

E-mail address: smeroueh@iupui.edu (S.O. Meroueh).

sive cells including lung cancer.¹ uPAR is able to associate with multiple binding partners at the cell surface to promote extracellular matrix (ECM) degradation and signaling,² such as the urokinase-type plasminogen activator (uPA) and vitronectin. Despite its lack of transmembrane domain, the receptor has been shown to promote signaling through integrins,^{3–7} receptor tyrosine kinases (RTKs)^{8,9} and GPCRs.¹⁰ In lung cancer cells, uPAR not only mediates signaling via integrins,¹¹ it also promotes invasion and degradation of the ECM by serving as a docking site to uPA and focusing proteolysis to the pericellular milieu.¹² In vivo, studies have shown that inhibition of uPAR activity reduces lung tumor growth and metastasis.^{13–15} In patient samples, uPAR serves as a strong prognostic factor for non-small cell lung cancer (NSCLC).¹⁶

The urokinase system has been implicated in nearly every step of tumor formation and progression, including tumorigenesis,¹⁷ cell proliferation,^{18–20} cell migration,^{21,22} adhesion,^{2,19} angiogenesis,^{23,24} and invasion.^{19,20,25,26} Hence, blocking the uPAR–uPA interaction is expected to result in significant impairment of metastasis. Peptides and antibodies have been developed to inhibit the tight protein interaction between uPAR and uPA.²⁷ However, the development of small molecules that abrogate this interaction remains

challenging given the tight nature of the binding.^{28–30} Recently, we reported the discovery of a small molecule (IPR-456; **1**) that binds to uPAR at sub-micromolar affinity (0.3 μM) and blocks its interaction with the amino-terminal fragment of uPA (uPA_{ATF}) with an IC₅₀ of 10 μM .³¹ The compound was discovered by virtual screening of a commercial library docked to multiple structures obtained from MD simulations. Cellular studies revealed that the compound inhibited MDA-MB-231 breast cancer cell invasion.

Here, we characterize a large number of derivatives of **1** from (i) commercial sources, and (ii) synthesis driven by rational design. Structure-based computational studies using molecular docking, explicit-solvent molecular dynamics (MD) simulations, and free energy calculations afforded a structure–activity study that uncovered the structural basis for inhibition. Cellular studies in NSCLC cell lines were carried out to assess the effect of two derivatives on cell invasion, migration, adhesion and proliferation. Further insight into the mechanism of action for the compound was assessed with protease activity and signaling studies probing ERK, Src, and FAK signaling.

2. Results

2.1. A cheminformatics search for derivatives

Starting with the structure of **1** (Scheme 1) a ligand-based similarity search of the ZINC chemical library³² identified 127 derivatives that share the core structure of the parental molecules. These derivatives were purchased and tested for inhibition of uPAR binding to uPA_{ATF}, using an ELISA that we previously developed.³¹ Among the 127 compounds tested at 50 μM , 15 had inhibitory activity (Fig. 1A). A concentration-dependent study confirmed these results (Fig. 1B). IC₅₀ values for 13 compounds that showed concentration-dependent inhibition—ranged from 5 μM for **3k** (IPR-824) to 100 μM for **3i** (IPR-809) (Table 1).

The aforementioned 127 derivatives had a common anthraquinone core with rings A, B and C (Scheme 1). Among these, the substituents at C2 and C4 varied considerably. It is interesting that the active derivatives possessed a carboxylate group at C4, either as part of a benzoic acid substituent (**3a–d**, **3i**, and **3k**), or appended to a chain that ranges from one to three carbon atoms in length (**3e–h**, **3j** and **3l**). The highest potency compound in the former category is **3k** (IPR-824), and in the latter category it is **3e** (IPR-664). *ortho*-, *meta*-, and *para*-carboxylates showed similar activity suggesting that the carboxylate can be positioned anywhere on the ring. But the *m*-carboxylate showed higher inhibition, for example, **3k** is more potent than **3c** (IPR-661). The C2 substituents for active compounds consisted primarily of hydrophobic five- and six-membered pyrrolidine and piperidine rings, except for **2** (IPR-803), which bears a seven-membered azepane ring. The piperidine rings have one or two methyl appendages, but for **3h** (IPR-804), which contains an ethylester moiety, while **3i** is a piperidinone derivative. Interest-

ingly, these two compounds were the weakest inhibitors. Comparison of **3b** (IPR-660) and **3k** (IPR-824) reveals that the total number of methyl groups on the six-membered piperidine ring had no effect on affinity.

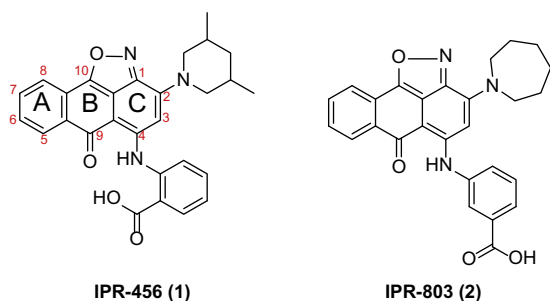
To gain insight into the direct binding of compounds to uPAR, we take advantage of the red-shifted fluorescence of the compounds and employ fluorescence polarization to study their interaction with uPAR. A concentration-dependent study was performed for eight compounds (Fig. 1D). Among them, seven (**3b–d**, **3f**, **3i**, **3m**, and **3n**) bind to uPAR with equilibrium constants ranging from 0.4 to 0.7 μM . These values are similar to those that we measured for **1** in the past (0.3 μM).³¹ Compound **3o** (IPR-632) showed no binding at the submicromolar concentrations considered in the FP assay. Despite its lack of activity in the ELISA, **3n** showed strong activity in the FP assay. This suggests that the compound is binding to uPAR, but is not able to displace the full protein interaction. This is due to the lack of a carboxylate moiety at C4 of the anthracene ring system, which we had earlier found to be critical for inhibition of the protein interaction. The benzoic acid ester lacks the charge on the benzoate group of the parent compound, which is likely responsible for its lack of activity.

2.2. Design and synthesis of derivatives

To study the role of the functional groups that did not vary in the commercial set of inhibitors, we resorted to synthesis of a set of derivatives (Schemes 2–6). Analogs of 1-hydroxyanthraquinone were prepared (Scheme 5). The Diels–Alder cyclization of 5-hydroxy-1, 4-naphthoquinone (**12**) and substituted butadienes afforded the cycloaddition products (**13a–c**) employing aluminum chloride as a catalyst.³³ Bromination of the Diels–Alder adduct was carried out using standard conditions of sodium acetate in refluxing acetic acid.³⁴ Arylamination of brominated adduct (**14a–c**) at the *p*-bromine in relation to the hydroxyl group was accomplished with Ullmann coupling conditions to give the required derivatives (**15a–c**).³⁵ Various alkylations (Schemes 2–4) at the hydroxyl group were accomplished using standard conditions, namely benzyl (**6**), isopropyl (**9**), and methyl (**11**) protection in order to probe the S4 pocket.^{36,37}

The replacement of the piperidine ring of **1** by a bromine group in **16** (IPR-630) resulted in little effect on activity. Further probing of the parental structure by opening the isoxazole ring of **1** also led to little impact on inhibition. The role of the primary amine that is created as a result of the ring opening was investigated in **10** (IPR-861) by replacing the amine with a hydroxyl moiety. The activity of **10** was identical to that of **17** (IPR-855) and slightly higher than **16**. This indicates that the amine group is neutralized upon binding, as it is unlikely that the change from a charged to a neutral group would not have an effect on activity. Neutral amines are often observed in a hydrophobic environment. To further probe the pocket occupied by this group, we designed and synthesized additional derivatives of **17**, namely **6** (IPR-863), **9** (IPR-864), and **11** (IPR-860). **11** bears a methoxy group, and an *o*-carboxylate. **6** and **9** possess a benzyloxy, and an isopropoxy group instead of the hydroxyl moiety. A concentration-dependent study showed significant loss of activity for **6** by nearly an order of magnitude, suggesting that the pocket for this group is not large enough to accommodate the benzyloxy group (Fig. 1C). However, the isopropoxy bearing **9** did show some inhibition (IC₅₀ = 30 μM), but was still weaker by threefold than its parent **17**. It was a surprise that **11** (IPR-860) showed no inhibition up to 100 μM despite the smaller methoxy substituent compared with the isopropoxy group of **9**. It is possible that the *o*-carboxylate of **11** combined with the methoxy group resulted in a loss of activity in a cooperative manner.

Finally, the role of the aromatic A-ring was studied through the introduction of methyl groups at A6 and A7. Two derivatives,



Scheme 1.

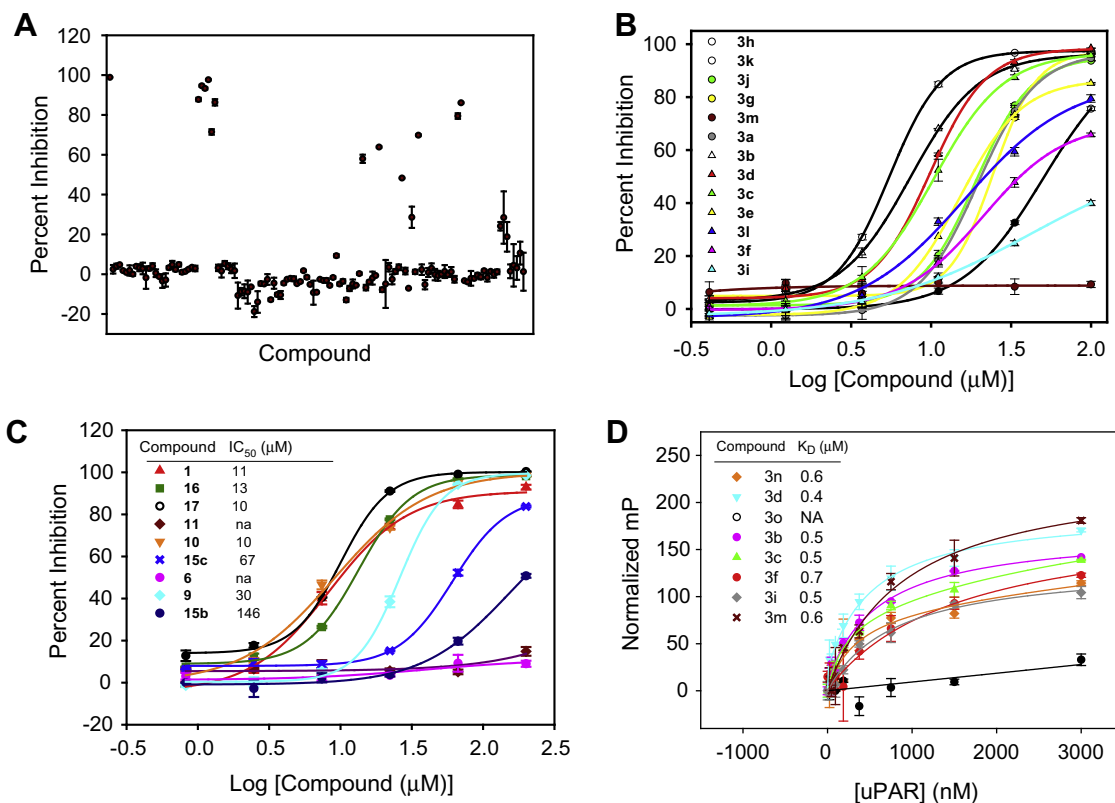


Figure 1. (A) Screening of 127 compounds that emerged from a similarity search of the ZINC chemical library based on the structure of **1**. Compounds were tested at a single concentration of 50 μM. (B) A concentration-dependent study of hit compounds obtained from commercial databases. Structure and inhibition constants are provided in Table 1. (C) A concentration-dependent study using our ELISA for compounds that were synthesized in this work. (D) binding affinity (K_D) of compounds using fluorescence polarization measured at a fixed concentration of compound and increasing concentration of uPAR.

namely **15b** (IPR-865) and **15c** (IPR-862), were prepared to contain a methyl group at A7 (**15b**), or two methyl groups, one at A6 and another at A7 (**15c**). It is interesting both of these compounds showed weaker inhibition than the parent, with IC_{50} of 146 and 67 μM, respectively (Fig. 1C). This suggests that the methyl groups cause steric clashes that prevent the compound from adopting the binding mode required for tight binding and inhibition of the protein interaction. This suggests that small alterations to the structure at the A ring significantly impair the compound's ability to inhibit the protein–protein interaction.

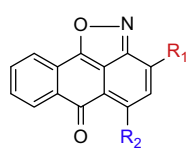
2.3. Structure-based computational study of binding mode

An analysis of the three dimensional structure of compounds in complex with uPAR could help explain changes in activity that were observed as a result of chemical modification of the parent compound. Short of a crystal structure, structure-based computational tools such as docking, molecular dynamics simulations (MD), and free energy calculations can be used not only to predict binding mode, but also to provide insight into the physical basis for interaction, and inform future structure-based design efforts. Docking of **1** along with two of its derivatives (**2** and **3k**) to uPAR revealed three possible binding poses (BP1, BP2, and BP3 as illustrated in Fig. 2A for **2**). The first binding mode (BP1) places the dimethyl piperidine (**1** and **3k**), and the azepane (**2**) substituent into the S2 cavity, while the aminobenzoic group of each compound is located at S3 (Fig. 2A and Fig. S1). In the second binding mode (BP2), the core anthraquinone structure is positioned similarly, but the carboxylate moiety of the aminobenzoic acid is buried into S3. In the third binding mode (BP3) the core anthraquinone structure adopts a similar position as BP1 and BP2, but the C2 and C4 substituents are flipped: C2 is ensconced into S4 and C3 is located in S2 (Fig. 2C). In each case,

the deeper S1 pocket in the cavity is occupied by the unsubstituted anthraquinone benzene A-ring.

To identify the most likely binding mode, we resorted to explicit-solvent MD simulations. The complex between the protein and the small molecule are placed into a large box of solvent molecules, and the trajectory of each atom is followed with respect to time, providing a detailed account of the motion of the complex. The snapshots along the trajectory not only provide insight on the stability of the ligand, but they can also be used to determine the free energy of binding using the MM-GBSA method as we have previously done.³¹ Starting with each binding mode of **1**, **2** and **3k**, we carried out a 5 × 10 ns explicit-solvent molecular simulation using the PMEMD module within the AMBER9 suite of programs.³² The structures collected over the course of the trajectory are used to measure the root-mean-square deviation (RMSD) of the atoms within the compound with respect to the first snapshot. As illustrated for **2** in Figure 2B, BP1 and BP3 showed lower RMSDs than BP2, suggesting that the binding modes are more stable. The RMSDs of the other compounds, namely **1** and **3k**, also revealed greater stability for BP1 and BP3 over BP2 (Supplementary data, Fig. S1).

To gain further insight on the stability of the binding mode of each compound, MM-GBSA calculations were performed to determine the free energy of binding and its components (Table 2): These include (i) a non-polar component ($\Delta E_{NP} = \Delta E_{VDW} + \Delta E_{SA}$), which comprises the sum of the van der Waals potential energy and non-polar solvation energy; (ii) a polar component ($\Delta E_{GBLE} = \Delta E_{COUL} + \Delta E_{GB}$), which consists of the Coulomb electrostatic energy and the Generalized-Born solvation energy; (iii) an entropy component ΔS_{NM} (Table 2). Interestingly, BP1 showed the most favorable free energy of binding for each compound, namely −16, −11, and −15 kcal/mol for **1**, **2**, and **3k**, respectively. BP2, the binding mode with the buried carboxylate, exhibited less stable values:

Table 1
Activity of purchased derivatives


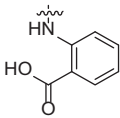
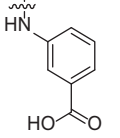
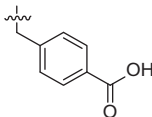
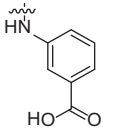
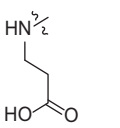
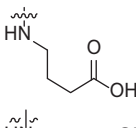
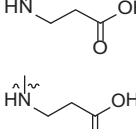
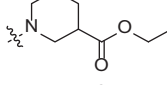
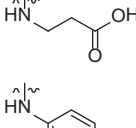
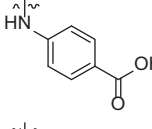
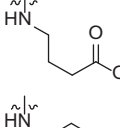
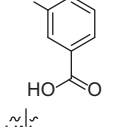
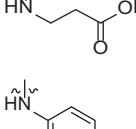
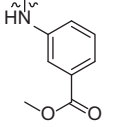
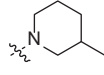
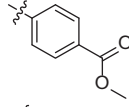
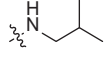
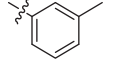
Compound	R ₁	R ₂	IC ₅₀ (μM)
3a (IPR-658)			21
3b (IPR-660)			7
3c (IPR-661)			11
3d (IPR-662)			10
3e (IPR-664)			18
3f (IPR-790)			36
3g (IPR-796)			24
3h (IPR-804)			51
3i (IPR-809)			>100
3j (IPR-811)			20
3k (IPR-824)			5
3l (IPR-663)			21
3m (IPR-853)			>100

Table 1 (continued)

Compound	R ₁	R ₂	IC ₅₀ (μM)
3n (IPR-646)			NA
3o (IPR-632)			NA

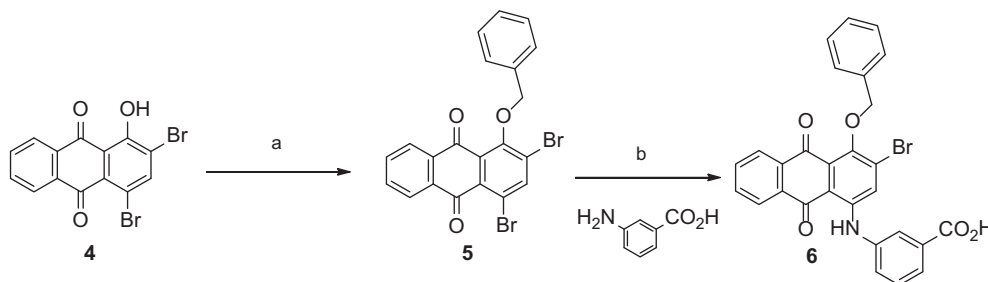
–12, –6, and –10 kcal/mol. Even less stable energies were found for BP3, with binding energies of –8, –10, and –8 kcal/mol for **1**, **2**, and **3k**. These results, combined with the lower RMSDs that were observed for this binding mode suggest that BP1 is the most likely binding mode for **1** and its derivatives.

MD simulations were also carried out for **3a**, **3i**, **6**, **9** and **15c**. RMSDs for **3a** (IPR-658) were lower than **3i** (Supplementary data Fig. S1). The greater stability of **3a** was reflected by the lower MM-GBSA binding free energy for **3i** (Table 2). This trend is consistent with our experimental data showing a higher affinity for **3a**. Compound **15c** (and **15b**) was conceived to probe the deep S1 cavity (Fig. 2A). However, the docked structures of these compounds reveal that the methyl groups at A6 and A7 prevented the compounds from adopting a similar binding mode to that of the active compounds. This was reflected in the higher free energy of binding (–8 kcal/mol) for this compound.

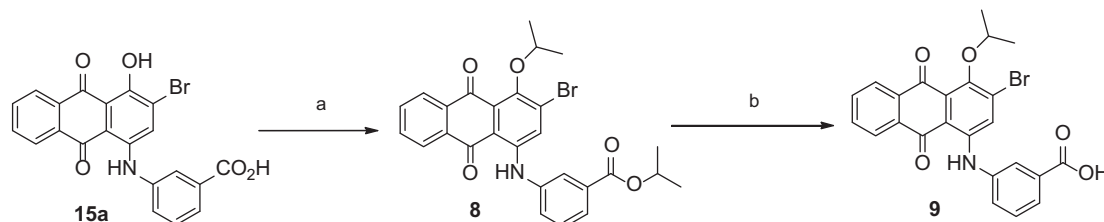
Compound **6** and **9** were designed to probe the cavity that accommodates nitrogen group in **16** and the hydroxyl group of **10**. The predicted structure of the compounds in the BP1 binding pose is shown in Figure S2. The anthracene core of **9** adopts a similar binding mode that is observed in **1** and other compounds. The isopropoxy group is ensconced into the smaller hydrophobic S4 pocket. The binding mode of **9** provided an explanation for the order of magnitude loss of affinity observed for this compound. The large benzyl group of **6** simply cannot be accommodated into the small S4 cavity (Fig. S2) and the aromatic ring is found to instead occupy the S3 binding pocket. This will likely result in severe clashes for compounds that have a large substituent at S3, such as **1** and **2**. The trend in the MM-GBSA free energies was consistent with our experimental data. Compound **6** was found to have the most unstable free energy (–7.5 kcal/mol; IC₅₀ = 30 μM) compared with **9** (–8.2 kcal/mol; IC₅₀ = 150 μM). Finally, despite its lack of activity in our biochemical studies, we attempted to predict a binding pose for **15c** (Fig. S2). Interestingly, we found that the two methyl groups on the compound prevented the anthracene core from adopting the same structure of the BP1 binding mode. Initially, these two methyl groups were added to extend into the deeper pocket of the S1 cavity of uPAR. Instead, it appears that the methyl groups clashed with the side chains of the residues at the entrance of the pocket, preventing the compound from adopting a productive binding mode for inhibition of the protein–protein interaction.

2.4. Inhibitors impair lung cancer invasion, migration and adhesion

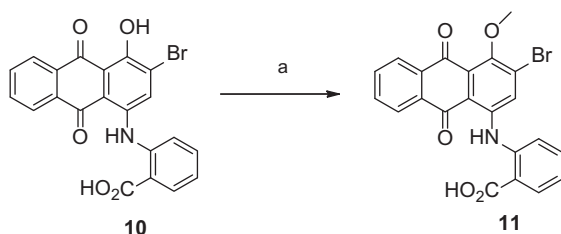
The importance of uPAR in promoting invasion and metastasis is well-documented. To study its role in NSCLC cell invasion, small interfering RNA (siRNA) knockdown of the receptor was carried out in A549, H1299 and H460, and confirmed by Western blot analysis (Fig. 3A). The effect on invasion was assessed using the Boyden chamber apparatus, revealing that the knockdown of uPAR impaired NSCLC invasion through the Matrigel layer (Fig. 3B and C). Nearly 40% inhibition of invasion was observed for each cell line. When **3k** is added to cells with silenced uPAR, an additional 30%



Scheme 2. Reagents and conditions: (a) K_2CO_3 , MEK/DMF (3:1), benzyl bromide; (b) $Cu(OAc)_2$, Cu, KOAc amyl alcohol, 150–160 °C.



Scheme 3. Reagents and conditions: (a) Ag_2O , $CHCl_3$, isopropyl iodide, rt; (b) 2 M NaOH (aq), MeOH, 70–80 °C.



Scheme 4. Reagents and conditions: (a) Ag_2O , $CHCl_3$, iodomethane, rt.

inhibition of invasion is observed (Fig. 3B and C). Previously, we had shown that **1** caused no additional effects on invasion when added to MDA-MB-231 cells with silenced uPAR.³¹ In this study, however, the silencing of uPAR in the lung cancer cell lines was not as complete, so that there may be some uPAR present at the surface. Hence, the greater level of inhibition observed for compound only could be due to inhibition of the residual uPAR receptors. Another possibility is that **3k** may bind to additional proteins given the structural differences with **1**. Hence **3k** may modulate the function of other proteins within the cell.

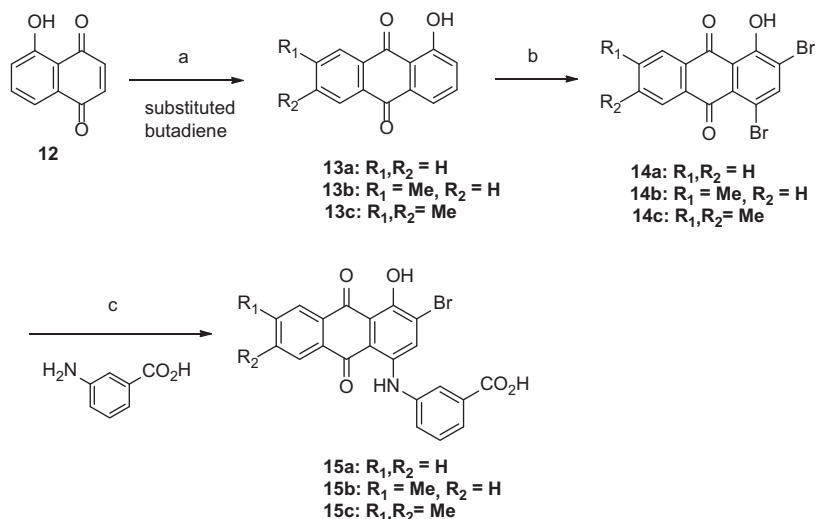
Further testing of invasion was done in a concentration-dependent study in the three NSCLC cell lines using compound **2**, whose binding and inhibition profile was thoroughly characterized previously.³¹ As shown in Figure 4A and B, **2** inhibited H1299, A549, and H460 invasion in a concentration-dependent manner with an IC_{50} that is estimated at about 10 μM . The inhibitor was more potent in H460 cells as evidenced by nearly complete inhibition at 50 μM . It showed less potency in H1299 cells, as illustrated by only 20% inhibition at 25 μM , compared with 80% for the other cell lines. The IC_{50} for inhibition of cell proliferation by **2** (Fig. 4F), which is nearly four times as large as the IC_{50} in our ELISA and invasion assays, suggesting that the effects on invasion are unrelated to cytotoxicity.

Studies have shown that uPAR engages cell surface integrins, which are responsible for cell attachment to ECM components and migration.^{3,5,7} First, we evaluated the effects of **2** on H1299 migration using the Boyden chamber apparatus (Fig. 4C and D). The compound inhibited migration in a concentration-dependent manner with an $IC_{50} = 50 \mu M$. The effects of the compounds on adhesion

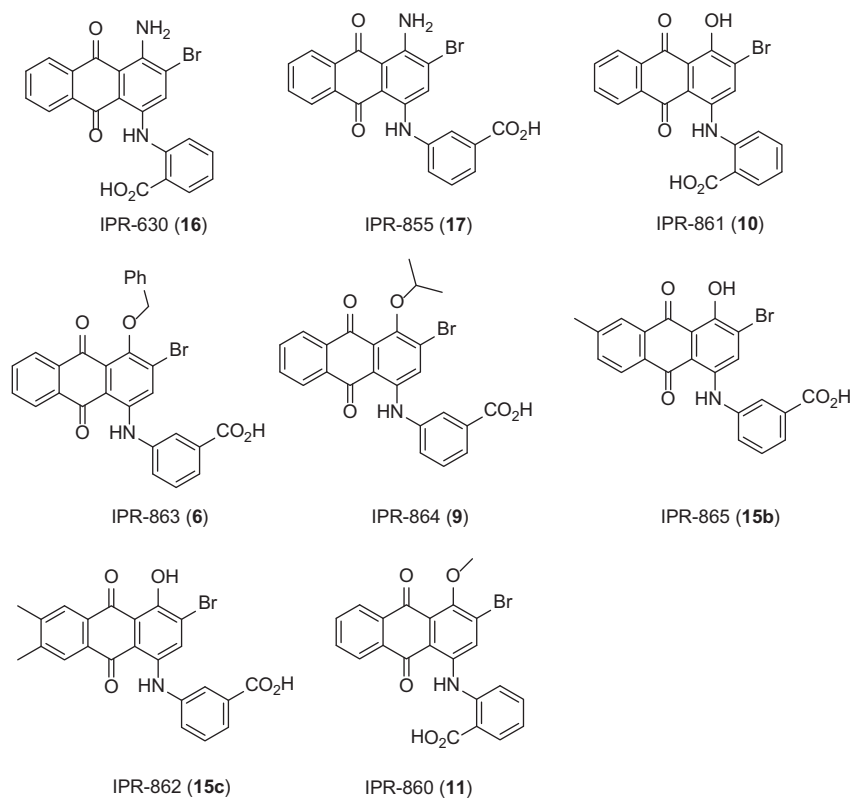
were also evaluated as we have done previously by measuring their effect on cell attachment to wells pre-coated with fibronectin and vitronectin.³⁸ Compound **2** inhibited adhesion in a concentration-dependent manner (Fig. 4E). The inhibition plateaued at about 40% for both vitronectin and fibronectin. The less significant effect on adhesion is not unexpected given that the compounds target the uPAR-uPA interface and do not directly impact the uPAR-integrin interface, which is located at a different site on uPAR.

2.5. Effect on proteolytic activity and signaling

The effect of **2** and its derivatives on invasion prompted us to assess whether the compounds affected uPA proteolytic activity in cells using a fluorimetric assay described previously.³⁹ While the small molecule does not directly bind to uPA, it is believed that the blocking of the uPAR-uPA interaction at the cell surface will likely result in less activation of uPA. Chloromethylketone (CMK) showed irreversible inhibition of uPA activity with nearly 50% and 60% inhibition at 10 and 50 μM of inhibitor, respectively (Fig. 5A). Compound **2** was also tested at these concentrations and showed 20% and 50% inhibition, similar to the activity seen for chloromethyl ketone. Another compound, namely UK122, which is thought to inhibit uPA catalytic activity, was also tested. However, significantly less activity of the compound was detected in our hands. A concentration of 400 μM had to be attained to detect nearly 50% of inhibition. It is interesting that IPR-803 inhibited the uPA proteolytic activity by nearly 50% at a concentration of 50 μM (Fig. 5A). Even at a concentration of 10 μM , IPR-803 inhibited by 25%. Unlike CMK or UK122, IPR-803 is not expected to directly inhibit uPA catalytic activity. Its effects are indirect, by blocking the binding of pro-uPA to uPAR, and therefore inhibiting its activation at the cell surface. uPA is known to lead to the activation of a number of proteinases, including matrix metalloproteinases (MMPs), which are well-known to degrade components of the ECM such as collagen. Numerous studies have targeted MMPs with small molecules as a strategy to block invasion.⁴⁰ To further probe the effect of **2** on proteolytic activity, matrix metalloproteinase activity is monitored with gelatin zymography in H1299 cells (Fig. 5B and C). Interestingly, an IC_{50} of nearly 50 μM is observed for **2**, which correlated well with the inhibition levels observed for uPA activity. It has been suggested in the past that activation of uPA results in plasmin acti-



Scheme 5. Synthesis of IPR-456 derivatives. Reagents and conditions: (a) AlCl₃, DCM, rt; (b) Br₂, NaOAc, AcOH, reflux; (c) Cu(OAc)₂, Cu, KOAc amyl alcohol, 150–160 °C.



Scheme 6. Synthesis of IPR-456 derivatives.

vation, which in turn leads to activation of MMPs. Hence, inhibition of uPA activity by **2** may affect MMP activation. Another possibility is that **2** inhibits uPAR-mediated signaling through integrins and other cell surface receptors that have been shown to promote activation. It is also possible that **2** and its derivatives inhibit other targets that affect MMP activity.

The interaction of uPAR with integrins and other cell surface receptors suggests that blocking these interactions may result in impairment of cell signaling. Three pathways in particular, namely ERK, FAK and Src have been implicated with integrin signaling. ERK signaling is responsible for promoting a number of cellular processes that include proliferation, differentiation and survival. FAK

is constitutively associated with β -integrin subunits of integrin receptors. Src, which is upstream of ERK, is also implicated in integrin signaling. Despite the fact that **2** inhibits the uPAR-uPA interaction, the effect of the compound on cell migration and adhesion prompted us to test its effect on cell signaling mediated by integrins by Western blot analysis. As shown in Figure 5D, there did not appear to be any effects on ERK phosphorylation. This is consistent with the fact that **2** binds to the uPA cavity, which is far from the integrin-binding site on uPAR.^{3,47} Therefore **2** is unlikely to impair the uPAR-integrin interaction, which has been shown to affect ERK signaling in previous studies using peptides and antibodies.^{3,12,41–49}

Structure-Based analysis

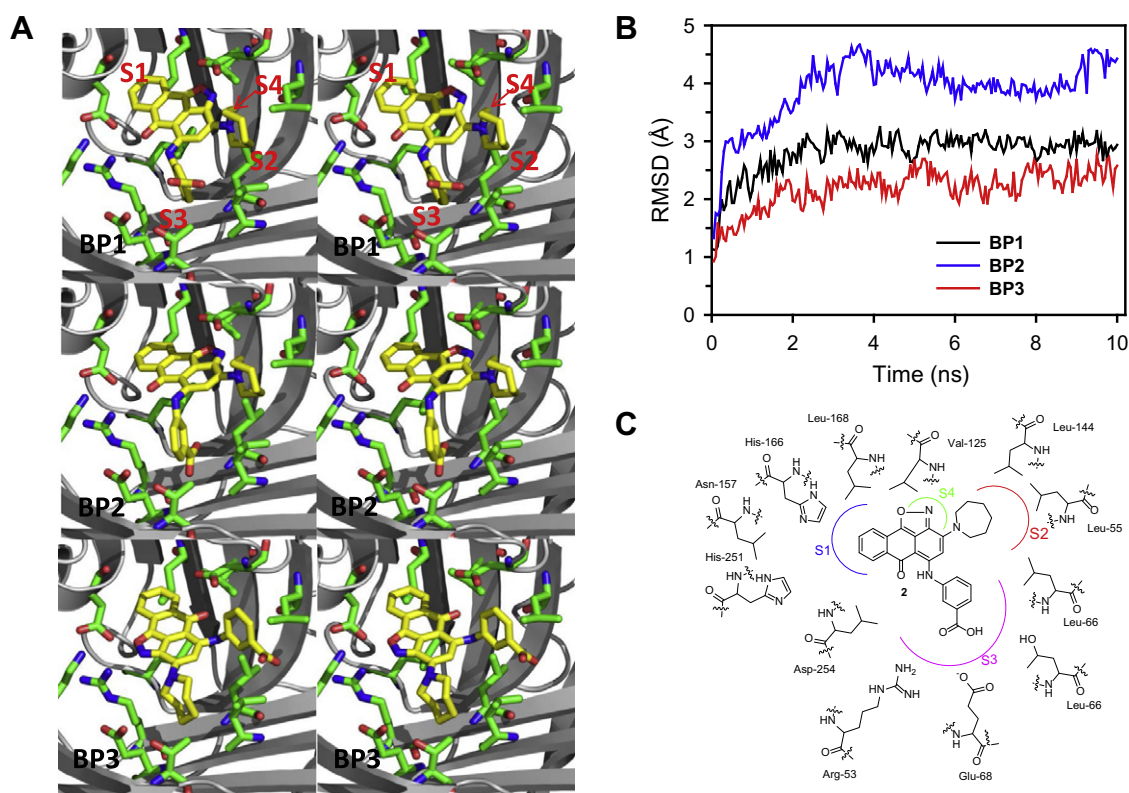


Figure 2. Structure-based analysis of uPAR/2 interactions. (A) Stereoview of the top three binding modes of compound **2** docked onto the uPA binding pocket on uPAR. The compound and the residues it interacts with were shown in sticks (carbon atoms in compound and protein were colored in yellow and green, respectively; nitrogens in blue and oxygens in red). The uPAR backbone was shown as grey ribbons. (B) The MD structures were aligned onto the first snapshot in the trajectory. The RMSD was calculated based on the heavy atoms of the compound. It was reported as the average of five independent trajectories in length of 10 ns. (C) The 2D schematic illustration of compound **2** interacting with residues on the uPAR pocket. Compound explores four sub-pockets (depicted with colored curves and named as S1, S2, S3 and S4, respectively) on the uPA binding pocket.

Table 2
Compound binding energy to uPAR calculated by MM-GBSA (in unit of kcal mol⁻¹)

Compound	Pose	ΔE_{VDW}	ΔE_{GBELE}	ΔE_{SA}	ΔE_{GBTOT}	$T\Delta S_{NM}$	ΔG_{GB}
1	BP1	-53.1 ± 0.2	21.0 ± 0.0	-6.2 ± 0.0	-39.2 ± 0.2	-22.9 ± 0.6	-16.3 ± 0.6
1	BP2	-49.8 ± 0.3	21.9 ± 0.0	-6.0 ± 0.0	-34.6 ± 0.3	-22.9 ± 0.6	-11.7 ± 0.6
1	BP3	-48.1 ± 0.2	26.1 ± 0.0	-5.8 ± 0.0	-28.6 ± 0.2	-20.8 ± 0.6	-7.8 ± 0.6
3k	BP1	-57.4 ± 0.2	24.8 ± 0.0	-6.2 ± 0.0	-39.6 ± 0.2	-25.0 ± 0.5	-14.7 ± 0.5
3k	BP2	-46.7 ± 0.5	21.2 ± 0.0	-5.8 ± 0.0	-31.9 ± 0.4	-22.3 ± 0.6	-9.6 ± 0.7
3k	BP3	-48.6 ± 0.2	25.2 ± 0.0	-5.8 ± 0.0	-29.9 ± 0.2	-22.4 ± 0.6	-7.5 ± 0.6
2	BP1	-53.8 ± 0.2	25.6 ± 0.0	-6.0 ± 0.0	-35.0 ± 0.2	-24.0 ± 0.6	-11.0 ± 0.6
2	BP2	-42 ± 0.4	20.2 ± 0.1	-5.6 ± 0.0	-28.1 ± 0.3	-21.7 ± 0.6	-6.4 ± 0.7
2	BP3	-49.8 ± 0.1	25.1 ± 0.0	-5.7 ± 0.0	-31.1 ± 0.1	-21.4 ± 0.6	-9.7 ± 0.6
3a	—	-45.6 ± 0.2	20.0 ± 0.0	-5.5 ± 0.0	-31.7 ± 0.2	-21.2 ± 0.6	-10.5 ± 0.6
3i	—	-40.6 ± 0.3	16.8 ± 0.0	-5.5 ± 0.0	-29.9 ± 0.3	-21.8 ± 0.6	-8.1 ± 0.7
15c	—	-47.1 ± 0.2	24.0 ± 0.0	-5.7 ± 0.0	-29.5 ± 0.1	-21.2 ± 0.6	-8.3 ± 0.6
6	—	-49.5 ± 0.2	27.1 ± 0.0	-6.1 ± 0.0	-29.3 ± 0.2	-21.8 ± 0.6	-7.5 ± 0.6
9	—	-48.4 ± 0.2	23.3 ± 0.0	-5.7 ± 0.0	-31.4 ± 0.2	-23.3 ± 0.6	-8.2 ± 0.6

ΔE_{VDW} , van der Waals potential energy; ΔE_{GBELE} , electrostatic contributions to the binding energy, of which the polar solvent contributions were calculated with Generalized Born equation; ΔE_{SA} , nonpolar solvent contribution to solvation free energy; ΔE_{GBTOT} , the sum of ΔE_{VDW} , ΔE_{GBELE} and ΔE_{SA} ; $T\Delta S_{NM}$, entropy calculated with normal mode analysis; ΔG_{GB} , the calculated free energy of binding using GB model.

2.6. Discussion

We build on our previous discovery of **1**, a small molecule that binds to uPAR and inhibits its protein interactions, to acquire a series of derivatives from commercial sources. These compounds varied strictly at C2 and C4, so synthesis was used to prepare an additional series of derivatives to probe the role of other groups on **1**. Beyond confirming the importance of the carboxylate moiety at C2, our activity data showed that the isoxazole ring of **1** is not critical for binding, and the amine group generated as a re-

sult of the ring opening does not play a significant role in binding. This was evidenced by the minimal loss of activity upon its conversion to a hydroxyl group. Further functionalization of this hydroxyl group to methoxy, isopropoxy and benzyloxy resulted in loss of inhibition suggesting that these groups engage a smaller pocket on uPAR. This was confirmed by extensive structure-based computational studies involving molecular docking, molecular dynamics simulations and free energy calculations. Functionalization of the A ring of **1** derivatives by introduction of methyl groups resulted in significant loss of activity. The predicted bind-

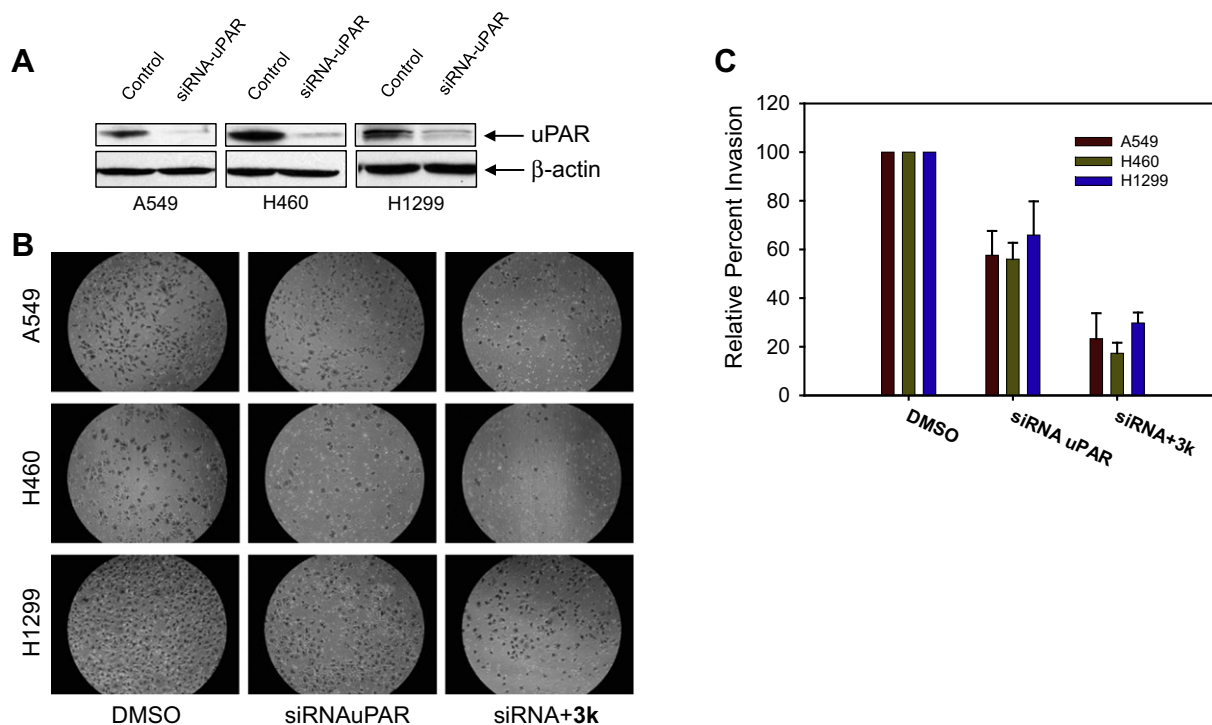


Figure 3. Invasion in the absence (control) or with **3k** for lung cancer cells with siRNA knockdown of uPAR. (A) H1299, H460 and A549 cells were transfected with siRNAs for uPAR or control siRNA (control). After 48 h, cells were lysed and analyzed by immunoblotting. (B) Representative experimental cells from control and in the presence of uPAR siRNA with or without **3k** were photographed for the Boyden chamber assays ($\times 200$) to illustrate the effect of **3k** on invasion as quantified in (C).

ing mode suggested that these groups clash with residues at the opening of the deeper S1 cavity on uPAR and prevent the compounds from adopting the necessary binding mode to inhibit the protein interaction. The computational studies revealed that the benzoic acid is ensconced within a hydrophobic pocket near the mouth of uPA binding cavity at the S3 binding pocket, engaging nearby Arg53 in a salt-bridge interaction. The substituent at C2 occupied another hydrophobic, but more solvent-exposed pocket on uPAR (S2). Cellular assays were performed to assess the activity of **2** in NSCLC cell lines. Compound **2** was shown to block lung cancer cell invasion in a concentration-dependent manner. The compound also inhibited lung cancer cell migration in a concentration-dependent manner and moderately inhibited adhesion suggesting a potential effect on the interaction between uPAR and integrins. However, signaling studies revealed that the compounds did not affect ERK, FAK or Src signaling, signifying that **2** may not be affecting integrin signaling. The effects observed on adhesion and migration could therefore be indirect, perhaps due to inhibition of the breakdown of the ECM, providing less space for the cells to migrate. The lack of effect on ERK signaling, which is affected by a large number of proteins, suggests that the compounds are specific to the uPAR-uPA interaction. Future efforts are concentrating on further improving the potency of **2** in tumor invasion and metastasis.

3. Materials and methods

3.1. Cell culture

H1299 and H460 cells were cultured in RPMI-1640 medium (Cellgro, Manassas, VA). A549 cells were cultured in Dulbecco's Modified Eagle Medium (Cellgro, Manassas, VA). Each medium was supplemented with 10% FBS and 1% penicillin/streptomycin in a 5% CO₂ atmosphere at 37 °C.

3.2. Reagents

Phospho-p44/42 MAPK and p44/42 MAPK, phospho-FAK (Tyr397), FAK; phospho-Src family (Tyr416) and Src antibodies were purchased from Cell Signaling Technology, Inc. (Danvers, MA). Actin antibody, uPAR siRNA and control siRNA were from Santa Cruz Biotechnology (Santa Cruz, CA). UK122 and Glu-Gly-Arg-chloromethyl ketone were from Calbiochem (San Diego, CA) and Z-Gly-Gly-Arg-AMC-HCl was from Bachem (Torrance, CA).

3.3. Microtiter-based ELISA

We used our previously developed microtiter-based ELISA.³¹ Briefly, medium- to high-binding microplates were coated and incubated for 2 h at 4 °C with 100 μ L of 2 μ g mL⁻¹ of uPA ATF in 1 \times PBS for immobilization. A 1:1 mixture of Superblock buffer in PBS (Thermo Fisher Scientific, Inc.) with 0.04 M NaH₂PO₄ and 0.3 M NaCl buffer was used for blocking. Following incubation and washing steps, serially diluted compounds were added with suPAR277 mixtures for 30 min. Following washing, biotinylated uPAR antibody (R&D Systems) in 1% BSA 1 \times PBS buffer was added to the wells (100 μ L/well) and incubated for 1 h to allow for the detection of bound uPAR. After that, streptavidin-peroxidase in 1% BSA 1 \times PBS buffer was added for 20 min. The signal obtained in the presence of TMB in phosphate-citrate buffer (0.2 M Na₂HPO₄ and 0.1 M citrate, pH 5) and hydrogen peroxide was stopped by adding H₂SO₄ solution and detected using an EnVision® Multi-label Plate Reader (PerkinElmer).

3.4. Proliferation assay

Cells were cultured at 37 °C in 10% FBS-DMEM or RPMI-1640 medium containing various amounts of compounds. 20 mM compound stock in 100% DMSO was serially diluted and added into

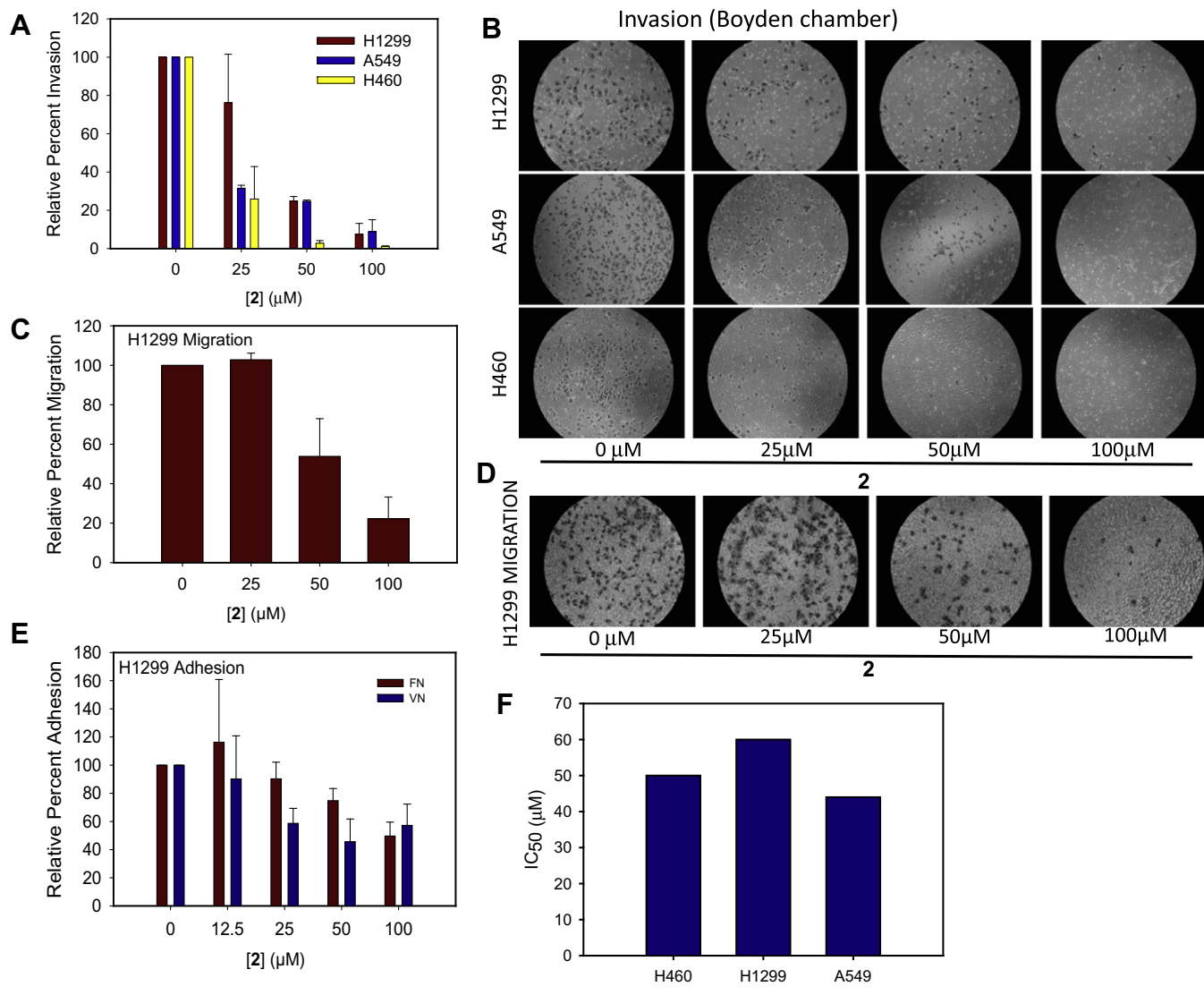


Figure 4. Compound **2** blocks invasion, migration and adhesion of H1299 cancer cells. (A, B) Invasion of H1299, H460 and A549 cells at increasing concentration of IPR-803, as indicated. Ten fields of each membrane were counted for cell numbers ($\times 200$). These data represent the average (SD of three independent experiments). (C, D) Migration of H1299 cells at increasing concentration of **2**, as indicated. Ten fields on each membrane were counted for cell numbers ($\times 200$). These data represent the average (SD of three independent experiments). (E) The adhesion of H1299 cells to ECM components fibronectin (FN) or vitronectin (VN) in the absence or presence of **2** are shown as indicated. The numbers of attached cells were quantified by MTT assay. (F) IC₅₀ for inhibition of A549, H460, and H1299 cell proliferation by **2**.

each well of a 96-well plate. Then treated cells were incubated for 3 days. Viable cells were quantified by MTT assay at absorbance of 570 and 630 nm as described previously.^{50,51}

3.5. Invasion and migration assays

Assays were performed using BD BioCoat Matrigel Invasion Chamber (cat. 354480, BD Biosciences, Bedford, MA) and Corning Transwell Permeable Support (Cat 3422, Corning Incorporated, Corning, NY) as described previously.^{31,50,52,53} In brief, the under-surfaces of the inserts were coated with 30 $\mu\text{g}/\text{mL}$ of fibronectin (Sigma, F2006) in PBS at 4 °C overnight. The inserts were washed with PBS once. Serum-free medium (0.5 mL) was separately added to the upper and lower chambers to equilibrate at 37 °C, 5% CO₂ for 2 h. After starvation with serum-free DMEM for 4 h, subconfluent cells were trypsinized and resuspended in 0.1% FBS media. Five hundred microliters of 10% FBS media containing various concentrations of compounds or DMSO were added to the lower chambers.

5×10^4 cells in 500 μL (for invasion) or 250 μL (for migration) of 0.1% FBS media containing the same compounds or 1% DMSO (as control) were added to the upper chambers. We incubated the chambers for 16 h at 37 °C, 5% CO₂. Non-invaded or non-migrated cells were removed from the upper chamber with a cotton swab. The invaded or migrated cells were fixed with 100% methanol and then stained with Hematoxylin Stain Harris Modified Method (Fisher, SH30-500D). We washed the filters with water three times. Filters were air-dried, and the invaded or migrated cells were counted in ten randomly selected microscopic fields (200 magnification). The experiment was performed in triplicate per group and shown by mean \pm SD.

3.6. Adhesion assay

Quantitative cell adhesion assays were carried out as described previously^{7,31,50} in 96-well microtiter plates, which were coated with either 15 $\mu\text{g}/\text{mL}$ fibronectin (Sigma) or 15 $\mu\text{g}/\text{mL}$ vitronectin

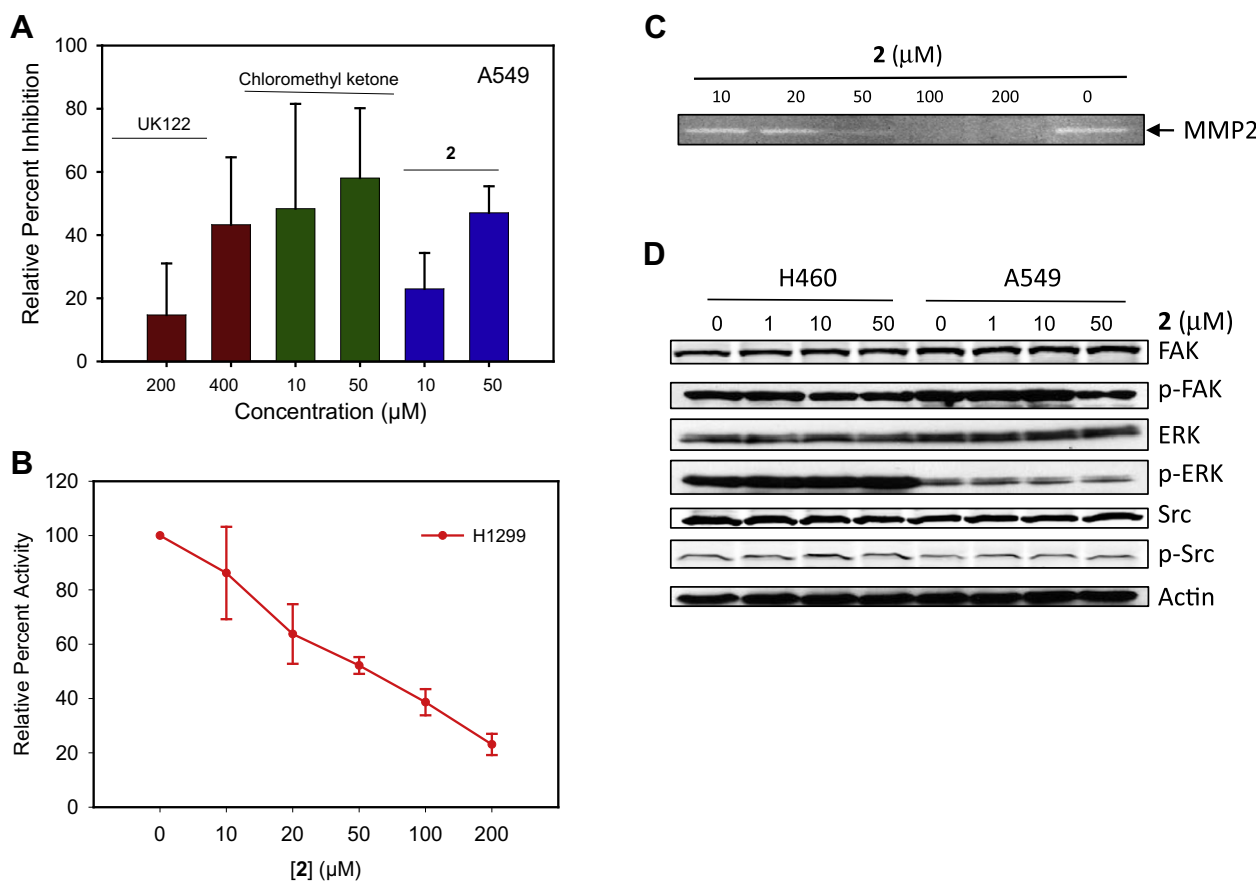


Figure 5. Proteolytic activity and signaling. (A) Fluorescence assays of cell surface-bound uPA activity in A549 cells. Cells were pre-incubated for 30 min with a range of concentrations of UK122, chloromethyl ketone or **2** on ice. Cells were washed, fluorogenic uPA-specific substrate was added and fluorescence measurements were recorded immediately. Initial rates of change in fluorescence after subtraction of background fluorescence (cells only) are presented as a percentage of control (no test compound added). Values represent means \pm SD ($n = 3$). (B, C) Effect on ECM degradation. Gelatin zymography analysis for H1299 cells with increasing concentration of **2** (D) Cell signaling study. H460 and A549 cells were treated with 1, 10 and 50 μ M compound(s) for 30 min, then immunoblotted with phospho-p44/42 MAPK and p44/42 MAPK, phospho-FAK (Tyr397), FAK; phospho-Src family (Tyr416), Src and actin, respectively.

(R&D Systems, Minneapolis, MN) overnight at 4 °C. Coated and uncoated control wells were blocked for 1 h with 2% bovine serum albumin (BSA) at 37 °C. Cells were split 1 day prior to the experiment to achieve a subconfluent culture. Briefly, H1299 cells were collected with trypsin, washed twice with serum-free medium, and 2×10^4 cells in 100 μ L of serum-free medium containing various compounds were added to each well, quadruplicate per group and incubated for 90 min at 37 °C. The wells were washed, and the number of adherent cells was quantified by MTT assay at 570 nm and 630 nm. The results were shown by means \pm SD.

3.7. Gelatin zymography

Zymography experiments were performed as described previously.^{50,54} H1299 cells were treated with different concentrations of **2** in serum free medium for 24 h, the conditioned medium was collected and concentrated by Amicon Ultra centrifugal filter units (Millipore, #UFC500324), and proteins were normalized and electrophoresed on 7.5% sodium dodecyl sulfate (SDS) polyacrylamide gels containing 1 mg/mL gelatin. After electrophoresis, the gel was washed twice in 50 mM Tris-HCl (pH 7.6) containing 5 mM CaCl₂ and 2.5% Triton X-100 for 30 min at room temperature and incubated in buffer that contained 50 mM Tris-HCl (pH 7.6), 200 mM NaCl, 10 mM CaCl₂, 1 mM ZnCl₂ at 37 °C for 36 h. Then, the gels were stained with 0.05% Coomassie brilliant blue (CBB) and destained with 30% methanol in 10% acetic acid. Areas of gel-

atolytic degradation appeared as transparent bands on the blue stained background of the gel. Data were quantified using Image J.

3.8. siRNA knockdown

H1299, H460 and A549 cells were transfected with uPAR siRNA or control siRNA for 48 h. Cells were then collected, and total cell lysates were prepared in standard RIPA extraction buffer containing aprotinin and phenyl-methyl-sulfonyl-fluoride as previously described.³¹ A 20 μ g sample of protein from these samples was separated by 12% SDS-PAGE and transferred to nitrocellulose membranes (Amersham, Arlington Heights, IL). The membranes were immunoprobed with antibodies against biotin-uPAR at 4 °C overnight. Next, membranes were treated with the appropriate HRP-conjugated secondary antibody and then developed according to enhanced chemi-luminescence protocol (Thermo Scientific, Rockford, IL). Membranes were stripped and reprobed with a monoclonal antibody against actin as a loading control.

3.9. Immunoblots

H460 and A549 cells were treated with 1, 10 and 50 μ M of IPR803 and 1% DMSO for 30 min. Cell lysates were harvested and separated by SDS-PAGE as mentioned above. For immunoblotting, the first antibody was phospho-p44/42 MAPK (Thr202/Tyr204), p44/42 MAPK; phospho-FAK (Tyr397), FAK; and phospho-Src

family (Tyr416) or Src mAb (Cell Signaling Technology, Inc., Danvers, MA) in 5% nonfat milk-TBST at 4 °C overnight. Secondary antibody consisted of goat anti-rabbit IgG or goat anti-mouse IgG HRP 1:3000 in 5% nonfat milk-TBST at room for 1 h and then developed as mentioned above.

3.10. Fluorometric HMW-uPA activity assays

Cell surface-bound uPA activity was measured using the fluorogenic substrate Z-Gly-Gly-Arg-AMC as previously described (De Souza 2011). The excitation wavelength of the substrate is 340 nm and the emission wavelength range is 460 nm. A549 cells were trypsinized, resuspended in cold PBS at 1×10^6 cells mL⁻¹ and incubated with test compounds for 30 min at 4 °C. Cells were then washed twice, transferred to a fluor plate, and PBS containing a final concentration of 0.1 mM Z-Gly-Gly-Arg-AMC as the fluorogenic substrate was added. Fluorescence emission was measured immediately using an Envision® Multilabel Plate Reader (PerkinElmer). Data was recorded at 2 min intervals over a period of 30 min. A control sample with no test compound was included. We calculated the rate of change in fluorescence min⁻¹ using the linear region of a graph where fluorescence was plotted against time.

3.11. MD simulations and analysis

The uPAR 3D structure was extracted from a uPAR crystal complex (PDB code: 3BT2). It was then prepared with the protein modeling package from Schrödinger, LLC (New York, NY) to add missing residues and atoms. Hydrogen atoms were added and optimized to a neutral environment. Disulfide bonds were created among Cysteine residues with short distance between sulfur atoms. The compounds were docked onto the uPA binding pocket on uPAR with autodock vina (version 1.1.2). The most favorable binding modes were returned. The compound binding modes were then visually inspected in PyMOL.⁵⁵ For 3 compounds (**1**, **2** and **3k**), three most probable binding modes for each compound were selected to subjected to explicit-solvent MD simulations. We retained the most commonly observed binding mode for other compounds. The following protocol for setting up and running the molecular dynamics simulations applies to all cases. The AMBER9⁵⁶ ff99SB force field for protein and GAFF⁵⁷ for small molecules were assigned. The atomic charges of the compound were determined by using the AM1-BCC methodology implemented in the antechamber program. The program Leap from the AMBER package was used to neutralize the complexes. The complexes of uPAR/compound were immersed in a box of TIP3P⁵⁸ water molecules such that no atom in the complex was within 14 Å from any side of the box. All bonds involving hydrogen atoms were constrained by using the SHAKE⁵⁹ algorithm, and a 2 fs time step was used. The particle mesh Ewald⁶⁰ method was used to treat long-range electrostatics. Water molecules were first energy minimized and equilibrated by running a short simulation with the complex fixed by using Cartesian restraints. This was followed by a series of energy minimizations in which the Cartesian restraints were gradually relaxed from 500 kcal Å⁻² to 0 kcal Å⁻², and the system was subsequently gradually heated to 300 K via a 48 ps molecular dynamics run. Production simulations were carried out in 5 independent runs, starting from the same structure but different initial atomic velocities. The PMEMD in AMBER9 was employed for production runs. MD snapshots were saved every 2 ps. A trajectory of 10 ns was collected for each run. The initial 2 ns on each trajectory was discarded to ensure only equilibrated structures are used in the analysis.

The method of MM-PBSA/GBSA for determining the binding free energy has been described in the past.^{61–63} It combines molecular mechanics, Generalized-Born electrostatics, surface-accessible cal-

culations, and normal mode analyses for energy and entropy calculation. In total, 500 snapshots were extracted evenly from the production trajectories for energy and entropy analysis. The MM-PBSA perl scripts in Amber⁵⁶ were employed to compute binding energy components and to decompose the binding energy on a per residue basis. The latter provides a useful insight on the relative importance of residues on the pocket to the binding of a ligand to uPAR.

3.12. Cloning, expression and purification of uPAR

We successfully cloned, expressed and purified uPAR. From 1 L of culture, we express nearly 12 mg of protein. Briefly, a truncated, soluble form of human uPAR (suPAR, amino acids 1–277) was expressed in stably transfected *Drosophila* S2 cells using the *Drosophila* Expression System (Invitrogen) and purified as described previously.

3.13. Fluorescence polarization

For direct binding studies of compounds using FP, varying concentrations of suPAR277 protein were titrated against intrinsically fluorescent compound with a final concentration of 1 μM in 1× PBS with 0.01% Triton X-100. The inhibitor-protein mix was incubated for 15 min to allow sufficient binding. Polarized fluorescence intensities were then measured using EnVision® Multilabel Plate Reader (PerkinElmer) with excitation and emission wavelengths of 531 and 595 nm, respectively. The reactions were carried out in duplicates.

3.14. Synthesis

All basic chemicals were purchased from commercially available sources and used as received. 1-Amino-2,4-dibromoanthraquinone and 5-hydroxy-1,4-naphthoquinone were purchased from Alfa Aesar. 1-hydroxyanthraquinone was purchased from TCI America. Column chromatography was carried out with silica gel (25–63 TCI Ament 6520 Accurate Mass Q-TOF instrument. ¹H NMR was recorded in CDCl₃, MeOH, or DMSO on a Bruker 500 MHz spectrometer. HP-LCMS was carried out on a Agilent 1100 LC/MSD fitted with a Eclipse XBD-C18 (4.6 × 150 mm) column eluting at 1.0 ml/min employing a gradient of (acetonitrile/methanol)/water (each containing 5 mM NH₄OAc) from 70% to 100% acetonitrile/methanol over 15 min and holding at 100% acetonitrile/methanol for 2 min. Chemical shifts are reported in ppm using residual CHCl₃, MeOH, or DMSO as internal references. Preparative HPLC was carried out using a X-Bridge Ost C18 2.5 μm column on a Waters 1525 Binary HPLC pump. All final compounds are 95% or greater purity from LC/MS, except for some intermediates or as otherwise indicated.

3.14.1. 1-Hydroxy-7-methylanthracene-9,10-dione and 1-hydroxy-6-methylanthracene-9,10-dione (**13b**)

5-Hydroxy-1,4-naphthoquinone (1.72 mmol, 300 mg) was dissolved in dry DCM (9 mL). The substituted butadiene (1.5 equiv) was added. Under Argon the solution was cooled to 0 °C and AlCl₃ (0.34 mmol, 45 mg) was added. The reaction was stirred at 0 °C for 1 h then warmed to ambient temperature. The reaction mixture was then heated to reflux overnight (~16 h). After the reaction was complete as judged by TLC, the reaction was cooled to ambient temperature and triethylamine (8.6 mmol, 1.20 mL) was added and left to stir vigorously overnight. The reaction was then washed with 1 N HCl, satd aq K₂CO₃ and brine. The organic layer was dried over anhydrous MgSO₄ and concentrated in vacuo. The crude solid was purified by column chromatography (eluting with 20% Et₂O/hexanes) to give the Diels–Alder product.³³ Yield: 123 mg (30%)

as a yellow solid. HRMS calcd for $C_{15}H_9O_3$ ($M-H$)⁻ 237.0557, found 237.0569. ¹H NMR (500 MHz, $CDCl_3$) δ 2.44 (s, 3H), 7.18 (ddd, $J = 8.51, 1.26, 0.63$ Hz, 1H), 7.47 (m, 1H), 7.56 (m, 1H), 7.68 (dt, $J = 7.57, 1.73$ Hz, 1H), 7.92 (s, 1H), 8.02 (dd, $J = 7.88, 1.58$ Hz, 1H), 12.47, 12.52 (syn and anti with respect to Me, 2s, 1H). ¹³C NMR (100 MHz, $CDCl_3$) δ 188.6, 188.2, 182.3, 181.8, 162.3, 145.8, 145.2, 136.5, 136.3, 135.3, 134.8, 133.3, 133.2, 132.8, 131.1, 130.7, 127.5, 127.4, 126.9, 124.1, 119.2, 116.0, 34.6, 31.5, 25.2, 22.6, 21.8, 20.6, 14.0.

3.14.2. 1-Hydroxy-6,7-dimethylanthracene-9,10-dione (13c)

Yield: 115 mg (26%) as a yellow solid. HRMS calcd for $C_{16}H_{11}O_3$ ($M-H$)⁻ 251.0714, found 251.0726. ¹H NMR (500 MHz, $CDCl_3$) δ 2.43 (s, 6H), 7.28 (dd, $J = 8.51, 0.95$ Hz, 1H), 7.64 (dd, $J = 7.88, 7.88$ Hz, 1H), 7.80 (dd, $J = 7.57, 1.26$ Hz, 1H), 8.03 (d, $J = 5.04$ Hz, 2H), 12.68 (s, 1H).

3.14.3. 2,4-Dibromo-1-hydroxy-7-methylanthracene-9,10-dione and 2,4-dibromo-1-hydroxy-6-methylanthracene-9,10-dione (14b)

To a stirred slurry of anthraquinone (1.0 equiv) and acetic acid (2 M) at ambient temperature was added NaOAc (3.0 equiv) followed by bromine (3.0 equiv). The reaction mixture was refluxed overnight (~16 h). The mixture was cooled to ambient temperature and diluted with water. The precipitate was filtered off and washed with additional water. The solid was dried in vacuo to give the desired brominated product.³⁴ Yield: 320 mg (quantitative) as a reddish-yellow solid. HRMS calcd for $C_{15}H_9Br_2O_3$ ($M+H$)⁺ 394.8913, found 394.8928. ¹H NMR (500 MHz, $CDCl_3$) δ 2.54 (d, $J = 3.78$ Hz, 3H), 7.60 (d, $J = 7.88$ Hz, 1H), 7.64 (d, $J = 7.88$ Hz, 1H), 8.06 (s, 1H), 8.15 (d, $J = 3.15$ Hz, 1H), 8.16 (d, $J = 3.15$ Hz, 1H) 8.19 (m, 1H), 8.21 (m, 1H), 14.04 (s, 1H), 14.09 (s, 1H).

3.14.4. 2,4-Dibromo-1-hydroxy-6,7-dimethylanthracene-9,10-dione (14c)

Yield: 228 mg (97%) as a reddish-yellow solid. HRMS calcd for $C_{16}H_{11}Br_2O_3$ ($M+H$)⁺ 408.9069, found 408.9075. ¹H NMR (500 MHz, $CDCl_3$) δ 2.42 (d, $J = 4.10$ Hz, 6H), 7.97 (d, $J = 4.41$ Hz, 2H), 8.16 (s, 1H), 14.09 (s, 1H).

3.14.5. 2,4-Dibromo-1-hydroxyanthracene-9,10-dione (14a)

Yield: 2.93 g (86%) as an orange solid. HRMS calcd for $C_{14}H_5Br_2O_3$ ($M-H$)⁻ 378.8611, found 378.8617. ¹H NMR (500 MHz, $CDCl_3$) δ 7.65–7.78 (m, 2H), 8.08 (s, 1H), 8.11–8.21 (m, 2H), 13.87 (s, 1H). ¹³C NMR (100 MHz, $CDCl_3$) δ 187.7, 180.2, 159.2, 145.6, 135.2, 133.9, 133.5, 131.2, 127.4, 126.5, 118.9, 117.3, 112.4, 104.4.

3.14.6. 3-((3-Bromo-4-hydroxy-9,10-dioxo-9,10-dihydroanthracen-1-yl)amino)benzoic acid (7)

To the dibromo anthraquinone derivative **14** (1.0 equiv) was added copper(II) acetate (0.3 equiv), copper dust (0.3 equiv), potassium acetate (2.0 equiv), aniline (3.0 equiv), and amyl alcohol (0.5 M). The reaction mixture was heated to 150–160 °C for 20–48 h. After the reaction was complete via TLC, the reaction was cooled to ambient temperature, ethanol was added with vigorous stirring, the precipitate was filtered off and washed with ethanol, then the solid was transferred to a dilute aqueous HCl solution and heated to 80–90 °C for 10 min and filtered again. The crude solid was left to air dry for 1 h and then dried in vacuo. The crude solid can be recrystallized in acetic acid to remove most of the impurities, but in certain cases prep HPLC is required for further purity.³⁵ Crude yield 1.01 g (88%) as a purple solid 3-((3-bromo-4-hydroxy-9,10-dioxo-9,10-dihydroanthracen-1-yl)amino)benzoic acid (**15a**). HRMS calcd for $C_{21}H_{11}BrNO_5$ ($M-H$)⁻ 435.9826, found 435.9851. ¹H NMR (500 MHz, $CDCl_3$) δ 7.38–7.43 (m, 1H), 7.49 (t,

$J = 8$ Hz, 1H), 7.84–7.95 (m, 5H), 8.39 (t, $J = 8.2$ Hz, 2H). LC/MS: rt = 4.62 min.

3.14.7. 2-((3-Bromo-4-hydroxy-9,10-dioxo-9,10-dihydroanthracen-1-yl)amino)benzoic acid (10)

Crude yield: 125 mg (37%) as a purple/blue solid. HRMS calcd for $C_{21}H_{11}BrNO_5$ ($M-H$)⁻ 435.9826, found 435.9855. ¹H NMR (500 MHz, $CDCl_3$) δ 7.12–7.19 (m, 1H), 7.43–7.49 (m, 2H), 7.82–7.97 (m, 3H), 8.04 (s, 1H), 8.30–8.43 (m, 2H). LC/MS: rt = 3.68 min.

3.14.8. 3-((3-Bromo-4-hydroxy-6-methyl-9,10-dioxo-9,10-dihydroanthracen-1-yl)amino)benzoic acid (15b)

Crude yield: 68 mg (60%) as a purple solid. HRMS calcd for $C_{22}H_{13}BrNO_5$ ($M-H$)⁻ 449.9983, found 450.0000. ¹H NMR (500 MHz, $CDCl_3$) δ 2.55, 2.56 (2s syn and anti with respect to hydroxyl group, 4H), 7.36–7.41 (m, 1H), 7.48 (t, $J = 7.8$ Hz, 1H), 7.69 (d, $J = 8$ Hz, 0.58H), 7.74 (d, $J = 8$ Hz, 1H), 7.81–7.90 (m, 3H), 8.16–8.20 (m, 1H), 8.26 (t, $J = 7.6$ Hz, 1H). LC/MS: rt = 5.04 min.

3.14.9. 3-((3-Bromo-4-hydroxy-6,7-dimethyl-9,10-dioxo-9,10-dihydroanthracen-1-yl)amino)benzoic acid (15c)

Crude yield: 39 mg (35%) as a purple solid. HRMS calcd for $C_{23}H_{15}BrNO_5$ ($M-H$)⁻ 464.0139, found 464.0159. ¹H NMR (500 MHz, MeOD) δ 2.21 (s, 1H), 2.46 (d, $J = 4$ Hz, 6H), 7.36–7.38 (m, 1H), 7.48 (t, $J = 8$ Hz, 1H), 7.78 (s, 1H), 7.84 (d, $J = 7.5$ Hz, 1H), 7.88 (s, 1H), 8.07 (app d, $J = 3.5$ Hz, 2H). LC/MS: rt = 6.43 min.

3.14.10. 2-((4-Amino-3-bromo-9,10-dioxo-9,10-dihydroanthracen-1-yl)amino)benzoic acid (16)

1-Amino-2,4-dibromoanthraquinone (0.13 mmol, 50 mg), copper carbonate (0.03 mmol, 4 mg), potassium acetate (0.46 mmol, 45 mg), and anthranilic acid (0.14 mmol, 19 mg) were refluxed for 12 h at 140 °C. The reaction was cooled to 80 °C and methanol was added. The blue solid was filtered off, washed with methanol, and air dried. The crude solid was recrystallized from acetic acid to give a bluish solid (46 mg, 81%).⁶⁴ HRMS calcd for $C_{21}H_{14}BrN_2O_4$ ($M+H$)⁺ 437.0137, found 437.0143. ¹H NMR (500 MHz, DMSO) δ 3.37 (s, 1H), 5.74 (s, 1H), 7.07 (t, $J = 7.09$ Hz, 1H), 7.41 (d, $J = 7.88$ Hz, 1H), 7.52 (t, $J = 6.94$ Hz, 1H), 7.84 (s, 2H), 7.95 (m, 2H), 8.19 (d, $J = 8.20$ Hz, 2H), 12.17 (s, 1H), 13.13 (s, 1H). ¹³C NMR (100 MHz, DMSO) δ 54.9, 110.5, 115.4, 119.7, 120.1, 120.5, 121.6, 126.0, 130.1, 131.8, 133.2, 133.3, 133.9, 133.5, 133.6, 136.9, 141.8, 144.5, 167.8, 182.7, 182.8. LC/MS: rt = 2.06 min.

3.14.11. 3-((4-Amino-3-bromo-9,10-dioxo-9,10-dihydroanthracen-1-yl)amino)benzoic acid (17)

To 1-amino-2,4-dibromoanthraquinone (2.62 mmol, 1 g) was added copper (II) acetate (0.79 mmol, 143 mg), copper dust (0.79 mmol, 50 mg), potassium acetate (5.24 mmol, 514 mg), 3-aminobenzoic acid (3.93 mmol, 539 mg), and amyl alcohol (5 mL). The reaction mixture was heated to 150–160 °C for 24 h. After the reaction was complete via TLC, the reaction was cooled to ambient temperature, ethanol was added with vigorous stirring, the precipitate was filtered off and washed with ethanol, then the solid was transferred to a dilute aqueous HCl solution and heated to 80–90 °C for 10 min and filtered again. The crude solid was left to air dry for 1 h and then dried in vacuo. The crude solid can be recrystallized in acetic acid to remove most of the impurities. Crude yield: 413 mg (36%), bluish solid. HRMS calcd for $C_{21}H_{12}BrNO_5$ ($M-H$)⁻ 434.9986, found 435.0011. ¹H NMR (500 MHz, $CDCl_3$) δ 7.33 (d, $J = 7$ Hz, 1H), 7.47 (d, $J = 8$ Hz, 1H), 7.76–7.93 (m, 7H), 8.31–8.38 (m, 2H). LC/MS: rt = 3.28 min, purity = 87%.

3.14.12. 2-((3-Bromo-4-methoxy-9,10-dioxo-9,10-dihydroanthracen-1-yl)amino)benzoic acid (11)

To a mixture of 2-((3-bromo-4-hydroxy-9,10-dioxo-9,10-dihydroanthracen-1-yl)amino)benzoic acid (0.11 mmol, 50 mg) and silver(I) oxide (0.22 mmol, 51 mg) in chloroform (1 mL) was added iodomethane (0.33 mmol, 21 μ L). The mixture was stirred for 20 h at ambient temperature in the dark. Additional silver(I) oxide (0.11 mmol) and iodomethane (0.11 mmol) was then added and the stirring continued for another 20 h. After the reaction was complete as judged by TLC, the mixture was filtered through celite and the solvent removed in vacuo to give the crude product (31 mg, 62%) as a reddish solid.³⁷ HRMS calcd for $C_{22}H_{13}BrNO_5$ (M–H)[–] 449.9983, found 450.0007. ¹H NMR (500 MHz, CDCl₃) δ 3.93 (s, 3H), 7.57–7.61 (m, 2H), 7.83–7.92 (m, 4H), 7.99 (br s, 1H), 8.04–8.08 (m, 1H), 8.20–8.34 (m, 3H). LC/MS: rt = 11.81 min, purity = 91%.

3.14.13. 3-((3-Bromo-4-isopropoxy-9,10-dioxo-9,10-dihydroanthracen-1-yl)amino)benzoic acid (9)

To a mixture of 3-((3-bromo-4-hydroxy-9,10-dioxo-9,10-dihydroanthracen-1-yl)amino)benzoic acid (0.23 mmol, 100 mg) and silver(I) oxide (0.46 mmol, 107 mg) in chloroform (2 mL) was added 2-iodopropane (0.69 mmol, 69 μ L). The mixture was stirred for 20 h at ambient temperature in the dark. Additional silver(I) oxide (0.23 mmol) and 2-iodopropane (0.23 mmol) was then added and stirred for another 20 h. After the reaction was complete as judged by TLC, the mixture was filtered through Celite and the solvent removed in vacuo to give the dialkylated crude product (50 mg, 45%). The dialkylated crude material was hydrolyzed in 2 M aqueous NaOH (140 μ L) and methanol (1 mL). Methanol was removed in vacuo and the solid residue was acidified to pH 2 to give the monoalkylated crude product (35 mg, 76%) as a reddish solid. HRMS calcd for $C_{24}H_{17}BrNO_5$ (M–H)[–] 478.0296, found 478.0320. ¹H NMR (500 MHz, MeOH) δ 1.29 (s, 1H), 1.36 (d, J = 6 Hz, 6H), 4.41–4.46 (m, 1H), 7.40–7.41 (m, 1H), 7.49 (t, J = 8 Hz, 1H), 7.73 (s, 1H), 7.81–7.89 (m, 3H), 7.91 (s, 1H), 8.19 (app d, J = 8 Hz, 1H), 8.29 (app d, J = 7 Hz, 1H). LC/MS: rt = 4.18 min.

3.14.14. 1-(Benzyloxy)-2,4-dibromoanthracene-9,10-dione (5)

To a solution of 2,4-dibromo-1-hydroxyanthracene-9,10-dione (0.51 mmol, 200 mg) in 3:1 methyl ethyl ketone/DMF (5 mL), potassium carbonate (0.77 mmol, 106 mg) was added followed by benzyl bromide (1.0 mmol, 119 μ L). The solution was refluxed for 20 h followed by quenching with slow addition of 1 M HCl (2.5 mL). Precipitate formed after cooling to 0 °C. The solid was filtered, washed with water, satd aqueous sodium carbonate, water, and brine to give 211 mg (88%) of a reddish solid. ¹H NMR (500 MHz, CDCl₃) δ 5.15 (s, 2H), 7.37 (t, J = 7.25 Hz, 1H), 7.43 (t, J = 7.25 Hz, 2H), 7.70 (d, J = 6.94 Hz, 2H), 7.77 (m, 2H), 8.18 (ddd, J = 8.99, 3.78, 3.63 Hz, 2H), 8.28 (s, 1H). ¹³C NMR (100 MHz, CDCl₃) δ 76.1, 117.6, 126.8, 126.9, 127.3, 128.5, 128.9, 130.0, 131.9, 133.4, 133.7, 134.0, 134.1, 136.0, 144.5, 155.5, 181.3, 181.9. HRMS calcd for $C_{21}H_{13}Br_2O_3$ (M+H)⁺ 470.9226, found 470.9232.

3.14.15. 3-((4-(Benzyloxy)-3-bromo-9,10-dioxo-9,10-dihydroanthracen-1-yl)amino)benzoic acid (6)

To 1-(benzyloxy)-2,4-dibromoanthracene-9,10-dione (0.11 mmol, 50 mg) was added copper(II) acetate (0.033 mmol, 6 mg), copper dust (0.033 mmol, 2 mg), potassium acetate (0.22 mmol, 22 mg), 3-aminobenzoic acid (0.33 mmol, 45 mg), and amyl alcohol (1 mL). The reaction mixture was refluxed for 20 h at 150–160 °C. After 20 h the reaction was cooled to ambient temperature, ethanol was added with vigorous stirring, the precipitate was filtered off and washed with ethanol, then the solid was transferred to a dilute aqueous HCl solution and heated to 80–90 °C for 10 min and filtered again. The crude solid was left to air dry for 1 h and then

dried in vacuo. A portion of the crude reddish solid (43 mg, 74%) was purified via prep HPLC. HRMS calcd for $C_{28}H_{17}BrNO_5$ (M–H)[–] 526.0296, found 526.0321. ¹H NMR (500 MHz, MeOH) δ 5.05 (s, 2H), 7.34–7.36 (m, 1H), 7.39–7.41 (m, 2H), 7.49 (t, J = 8 Hz, 1H), 7.68 (app d, J = 7 Hz, 2H), 7.45 (s, 1H), 7.82–7.90 (m, 3H), 7.90–7.91 (m, 1H), 8.22 (app d, J = 7 Hz, 1H), 8.30 (app d, J = 7 Hz, 1H), 8.55 (br s, 2H). LC/MS: rt = 5.89 min.

Acknowledgments

The research was supported by the National Institutes of Health (CA135380) (SOM), the INGEN grant from the Lilly Endowment, Inc. (SOM), by The Indiana University Melvin and Bren Simon Cancer Center Translational Research Acceleration Collaboration (ITRAC) (SOM), the Showalter Trust (SOM), by the Indiana University Biomedical Research Fund (SOM) and by the American Cancer Society Institutional Grant (SOM). Computer time on the Big Red supercomputer at Indiana University is funded by the National Science Foundation and by Shared University Research.

Supplementary data

Supplementary data associated with this article can be found, in the online version, at <http://dx.doi.org/10.1016/j.bmc.2012.06.002>.

References and notes

- Werle, B.; Kotzsch, M.; Lah, T. T.; Kos, J.; Gabrijelcic-Geiger, D.; Spiess, E.; Schirren, J.; Ebert, W.; Fiehn, W.; Luther, T.; Magdolen, V.; Schmitt, M.; Harbeck, N. *Anticancer Res.* **2004**, *24*, 4147.
- Andreasen, P. A.; Kjoller, L.; Christensen, L.; Duffy, M. J. *Int. J. Cancer* **1997**, *72*, 1.
- Wei, Y.; Tang, C. H.; Kim, Y.; Robillard, L.; Zhang, F.; Kugler, M. C.; Chapman, H. A. *J. Biol. Chem.* **2007**, *282*, 3929.
- Wei, Y.; Czekay, R. P.; Robillard, L.; Kugler, M. C.; Zhang, F.; Kim, K. K.; Xiong, J. P.; Humphries, M. J.; Chapman, H. A. *J. Cell Biol.* **2005**, *168*, 501.
- Simon, D. I.; Wei, Y.; Zhang, L.; Rao, N. K.; Xu, H.; Chen, Z. P.; Liu, Q. M.; Rosenberg, S.; Chapman, H. A. *J. Biol. Chem.* **2000**, *275*, 10228.
- Wei, Y.; Lukashev, M.; Simon, D. I.; Bodary, S. C.; Rosenberg, S.; Doyle, M. V.; Chapman, H. A. *Science* **1996**, *273*, 1551.
- Wei, Y.; Eble, J. A.; Wang, Z.; Kreidberg, J. A.; Chapman, H. A. *Mol. Biol. Cell* **2001**, *12*, 2975.
- Kiyan, J.; Kiyan, R.; Haller, H.; Dumler, I. *EMBO J.* **2005**, *24*, 1787.
- Liu, D.; Aguirre Ghiso, J.; Estrada, Y.; Ossowski, L. *Cancer Cell* **2002**, *1*, 445.
- Resnati, M.; Pallavicini, I.; Wang, J. M.; Oppenheim, J.; Serhan, C. N.; Romano, M.; Blasi, F. *Proc. Natl. Acad. Sci. U.S.A.* **2002**, *99*, 1359.
- Tang, C. H.; Hill, M. L.; Brumwell, A. N.; Chapman, H. A.; Wei, Y. *J. Cell Sci.* **2008**, *121*, 3747.
- Durisetti, S.; Goetz, D. H.; Hostetter, D. R.; LeBeau, A. M.; Wei, Y.; Craik, C. S. *J. Biol. Chem.* **2010**, *285*, 26878.
- Henneke, I.; Greschus, S.; Savai, R.; Korfei, M.; Markart, P.; Mahavadi, P.; Schermuly, R. T.; Wygrecka, M.; Sturzebecher, J.; Seeger, W.; Gunther, A.; Ruppert, C. *Am. J. Respir. Crit. Care Med.* **2010**, *181*, 611.
- Carriero, M. V.; Longanesi-Cattani, I.; Bifulco, K.; Maglio, O.; Lista, L.; Barbieri, A.; Votta, G.; Masucci, M. T.; Arra, C.; Franco, R.; De Rosa, M.; Stoppelli, M. P.; Pavone, V. *Mol. Cancer Ther.* **2009**, *8*, 2708.
- Rao, J. S.; Gondi, C.; Chetty, C.; Chittivelu, S.; Joseph, P. A.; Lakka, S. S. *Mol. Cancer Ther.* **2005**, *4*, 1399.
- Almasi, C. E.; Hoyer-Hansen, G.; Christensen, I. J.; Pappot, H. *APMIS* **2009**, *117*, 755.
- Shapiro, R. L.; Duquette, J. G.; Nunes, I.; Roses, D. F.; Harris, M. N.; Wilson, E. L.; Rifkin, D. B. *Am. J. Pathol.* **1997**, *150*, 359.
- Gandhari, M.; Arens, N.; Majety, M.; Dorn-Beineke, A.; Hildenbrand, R. *Int. J. Oncol.* **2006**, *28*, 1463.
- Liang, X.; Yang, X.; Tang, Y.; Zhou, H.; Liu, X.; Xiao, L.; Gao, J.; Mao, Z. *Oral Oncol.* **2008**, *12*, 23.
- Kondraganti, S.; Gondi, C. S.; McCutcheon, I.; Dinh, D. H.; Gujrati, M.; Rao, J. S.; Olivero, W. C. *Int. J. Oncol.* **2006**, *28*, 1353.
- Prager, G. W.; Breuss, J. M.; Steurer, S.; Olcaydu, D.; Mihaly, J.; Brunner, P. M.; Stockinger, H.; Binder, B. R. *Circ. Res.* **2004**, *94*, 1562.
- Schiller, H. B.; Szekeres, A.; Binder, B. R.; Stockinger, H.; Leksa, V. *Mol. Biol. Cell* **2009**, *20*, 745.
- Mignatti, P.; Rifkin, D. B. *Enzyme Protein* **1996**, *49*, 117.
- Rabbani, S. A.; Mazar, A. P. *Surg. Oncol. Clin. N. Am.* **2001**, *10*, 393.
- Subramanian, R.; Gondi, C. S.; Lakka, S. S.; Jutla, A.; Rao, J. S. *Int. J. Oncol.* **2006**, *28*, 831.

26. Kunigal, S.; Lakka, S. S.; Gondi, C. S.; Estes, N.; Rao, J. S. *Int. J. Cancer* **2007**, *121*, 2307.
27. Mazar, A. P. *Clin. Cancer Res.* **2008**, *14*, 5649.
28. Ploug, M.; Ellis, V. *FEBS Lett.* **1994**, *349*, 163.
29. Gardsvoll, H.; Gilquin, B.; Le Du, M. H.; Menez, A.; Jorgensen, T. J.; Ploug, M. *J. Biol. Chem.* **2006**, *281*, 19260.
30. Reuning, U.; Sperl, S.; Kopitz, C.; Kessler, H.; Kruger, A.; Schmitt, M.; Magdolen, V. *Curr. Pharm. Des.* **2003**, *9*, 1529.
31. Khanna, M.; Wang, F.; Jo, I.; Knabe, W. E.; Wilson, S. M.; Li, L.; Bum-Erdene, K.; Li, J.; Sledge, G. W.; Khanna, R.; Meroueh, S. O. *ACS Chem. Biol.* **2011**, *6*, 1232.
32. Irwin, J. J.; Shoichet, B. K. *J. Chem. Inf. Model.* **2005**, *45*, 177.
33. Elkazaz, S.; Jones, P. B. *J. Org. Chem.* **2010**, *75*, 412.
34. Jones, P. B.; Brinson, R. G.; Sarma, S.; Elkazaz, S. *Org. Biomol. Chem.* **2008**, *6*, 4204.
35. Ullmann, F.; Eiser, O. *Ber. Dtsch. Chem. Ges.* **1916**, *49*, 2154.
36. Sarma, S. J.; Jones, P. B. *J. Org. Chem.* **2010**, *75*, 3806.
37. Tietze, L. F.; Gericke, K. M.; Singidi, R. R.; Schuberth, I. *Org. Biomol. Chem.* **2007**, *5*, 1191.
38. Khanna, M.; Chelladurai, B.; Gavini, A.; Li, L.; Shao, M.; Courtney, D.; Turchi, J. J.; Matei, D.; Meroueh, S. *Mol. Cancer Ther.* **2011**, *10*, 626.
39. De Souza, M.; Matthews, H.; Lee, J. A.; Ranson, M.; Kelso, M. J. *Bioorg. Med. Chem.* **2011**, *19*, 2549.
40. Brown, S.; Meroueh, S. O.; Fridman, R.; Mobashery, S. *Curr. Top. Med. Chem.* **2004**, *4*, 1227.
41. Aguirre Ghiso, J. A.; Kovalski, K.; Ossowski, L. *J. Cell Biol.* **1999**, *147*, 89.
42. Aguirre-Ghiso, J. A.; Estrada, Y.; Liu, D.; Ossowski, L. *Cancer Res.* **2003**, *63*, 1684.
43. Aguirre-Ghiso, J. A.; Liu, D.; Mignatti, A.; Kovalski, K.; Ossowski, L. *Mol. Biol. Cell* **2001**, *12*, 863.
44. Ahmed, N.; Oliva, K.; Wang, Y.; Quinn, M.; Rice, G. *Br. J. Cancer* **2003**, *89*, 374.
45. Chaurasia, P.; Aguirre-Ghiso, J. A.; Liang, O. D.; Gardsvoll, H.; Ploug, M.; Ossowski, L. *J. Biol. Chem.* **2006**, *281*, 14852.
46. Chaurasia, P.; Mezei, M.; Zhou, M. M.; Ossowski, L. *PLoS One* **2009**, *4*, e4617.
47. Geetha, N.; Mihaly, J.; Stockenhuber, A.; Blasi, F.; Uhrin, P.; Binder, B. R.; Freissmuth, M.; Breuss, J. M. *J. Biol. Chem.* **2011**, *286*, 25663.
48. Ma, Z.; Webb, D. J.; Jo, M.; Gonias, S. L. *J. Cell Sci.* **2001**, *114*, 3387.
49. Wei, Y.; Yang, X.; Liu, Q.; Wilkins, J. A.; Chapman, H. A. *J. Cell Biol.* **1999**, *144*, 1285.
50. Wang, F.; Li, J.; Sinn, A. L.; Knabe, W. E.; Khanna, M.; Jo, I.; Silver, J. M.; Oh, K.; Li, L.; Sandusky, G. E.; Sledge, G. W.; Nakshatri, H.; Jones, D. R.; Pollok, K. E.; Meroueh, S. O. *J. Med. Chem.* **2011**, *54*, 7193.
51. Twentymann, P. R.; Luscombe, M. *Br. J. Cancer* **1987**, *56*, 279.
52. Albini, A.; Iwamoto, Y.; Kleinman, H. K.; Martin, G. R.; Aaronson, S. A.; Kozlowski, J. M.; McEwan, R. N. *Cancer Res.* **1987**, *47*, 3239.
53. Parkkila, S.; Rajaniemi, H.; Parkkila, A. K.; Kivela, J.; Waheed, A.; Pastorekova, S.; Pastorek, J.; Sly, W. S. *Proc. Natl. Acad. Sci. U.S.A.* **2000**, *97*, 2220.
54. Toth, M.; Fridman, R. *Methods Mol. Med.* **2001**, *57*, 163.
55. DeLano, W. L. *DeLano Scientific*; Palo Alto: CA, USA, 2002.
56. Case, D. A.; Darden, T. A.; Cheatham, T. E., III; Simmerling, C. L.; Wang, J.; Duke, R. E.; Luo, R.; Merz, K. M.; Wang, B.; Pearlman, D. A.; Crowley, M.; Brozell, S.; Tsui, V.; Gohlke, H.; Mongan, J.; Hornak, V.; Cui, G.; Beroza, P.; Schafmeister, C.; Caldwell, J. W.; Ross, W. S.; Kollman, P. A. University of California: San Francisco, 2004.
57. Wang, R.; Lu, Y.; Fang, X.; Wang, S. *J. Chem. Inf. Comput. Sci.* **2004**, *44*, 2114.
58. Jorgensen, W. L.; Chandrasekhar, J.; Madura, J. D.; Impey, R. W.; Klein, M. L. *J. Chem. Phys.* **1983**, *79*, 10.
59. Ryckaert, J. P.; Ciccotti, G.; Berendsen, J. J. C. *J. Comput. Phys.* **1977**, *23*, 15.
60. Darden, T.; York, D.; Pedersen, L. *J. Chem. Phys.* **1993**, *98*, 10089.
61. Srinivasan, J.; Cheatham, T. E.; Cieplak, P.; Kollman, P. A.; Case, D. A. *J. Am. Chem. Soc.* **1998**, *120*, 9401.
62. Kollman, P. A.; Massova, I.; Reyes, C.; Kuhn, B.; Huo, S. H.; Chong, L.; Lee, M.; Lee, T.; Duan, Y.; Wang, W.; Donini, O.; Cieplak, P.; Srinivasan, J.; Case, D. A.; Cheatham, T. E. *Acc. Chem. Res.* **2000**, *33*, 889.
63. Wang, J. M.; Morin, P.; Wang, W.; Kollman, P. A. *J. Am. Chem. Soc.* **2001**, *123*, 5221.
64. Ukponmwan, D. O.; Greenhaigh, M.; Peters, A. T. *J. Chem. Eng. Data* **1984**, *29*, 482.